Formation of Monomeric S100B and S100A11 Proteins at Low Ionic Strength[†]

Nicole M. Marlatt,[‡] Brian L. Boys,[§] Lars Konermann,[‡,§] and Gary S. Shaw*[,‡,§]

Department of Biochemistry, University of Western Ontario, London, Ontario N6A 5C1, Canada, and Department of Chemistry, University of Western Ontario, London, Ontario N6A 5B7, Canada

Received November 11, 2008; Revised Manuscript Received December 23, 2008

ABSTRACT: The S100 proteins comprise a group of EF-hand proteins that undergo a calcium-induced conformational change allowing them to interact with other proteins and produce a biological response. A unique feature of these proteins is the fact that they can form both homo- and heterodimers independent of calcium binding. The reported dissociation constants for several S100 proteins span a very large range, from 1−4 μM to ≪1 nM, suggesting that differing interface surface areas could govern the strength of the binding affinity. In this work, we examine the dimerization mechanism of S100B and S100A11 in the absence of calcium. Using electrospray mass spectrometry, we demonstrate that the monomer−dimer equilibrium in these S100 proteins is strongly dependent on the ionic strength of the solution. At higher ionic strengths (≥22 mM), both S100A11 and S100B exist predominantly as homodimers. For apo-S100A11, a K_{dimer} near 0.01 μM is estimated, while concentration-dependent experiments under these conditions show the K_{dimer} for apo-S100B must be even lower. In contrast, lowering the ionic strength results in the formation of monomeric proteins with poorer dimer propensity. For example, the estimated K_{dimer} for apo-S100A11 is more than 400 μM at 0.1 mM NH_4Ac. $^1H-^{15}N$ HSQC NMR experiments in combination with circular dichroism studies show that monomeric S100B and S100A11 proteins are α-helical and retain a significant amount of tertiary structure. Our results indicate that apo-S100B has at least a 10-fold stronger propensity to form dimers than does apo-S100A11 in line with a 400 Å^2 greater buried surface area for apo-S100B at its dimer interface. These experiments are the first to show that folded monomeric S100 proteins can be isolated, thus paving the way for future experiments aimed at examining the possible role of these monomers in folding and calcium signaling.

The S100 family comprises the largest group of human EF-hand calcium-binding proteins (for recent reviews, see refs *1* and *2*). Similar to traditional EF-hand calcium-binding proteins such as calmodulin and troponin C, most S100 proteins function through a calcium-induced conformational change that results in their interaction with a wide variety of target proteins, thereby leading to a biological response. For example, S100B can bind to tubulin, GFAP, and desmin to modulate the assembly of these cytoskeletal components (*3*−*5*). Similarly, calcium-bound S100A4 is involved in the regulation of cellular motility by interacting with myosin heavy chain II (*6*). Unlike calmodulin and troponin C, most S100 proteins have the ability to form homo- and heterodimers. Dimerization can occur both in the presence and in the absence of calcium. In some cases, including S100A1 and S100B (*7*) and S100A8 and S100A9 (*8*), heterodimers have been isolated from tissue.

The three-dimensional structures of several homodimeric S100 proteins have been determined, including S100B (*9*−*12*), S100A11 (*13, 14*), and S100A6 (*15*−*18*). These data have revealed that the proteins possess two helix−loop−helix calcium-binding sites within each subunit, comprised of helices I and II for site I and helices III and IV for site II with an extended linker region separating the two sites. A structural comparison of calcium-free (apo) and calcium-bound dimers has shown that calcium binding to S100B (*9*−*12, 19*), S100A6 (*15*−*18, 20*), S100A11 (*13, 14*), and S100A13 (*21*−*23*) results in a reorientation of helix III, liberating a hydrophobic surface that facilitates protein interactions. Further, the structures have provided important details about the dimer interface, which represents the most structurally conserved region in these proteins. This interface is formed from an X-bundle arrangement of helices I and IV from one monomer and helices I′ and IV′ from its partner. As a result, hydrophobic amino acids spaced at intervals of three to four residues are important for maintaining the S100 dimeric structure (*12, 24, 25*).

The formation of both homo- and heterodimeric S100 proteins indicates that exchange between subunits likely occurs in vivo. Indeed, it has been observed that S100B can interact with S100A1, S100A6, and S100A11 in yeast two-hybrid experiments (*26, 27*), suggesting that the subunit interchange of these proteins may be highly dynamic. In

[†] This work was supported by the Canadian Institutes of Health Research (G.S.S.), the Canada Research Chairs Program (G.S.S. and L.K.), and the Natural Sciences and Engineering Research Council of Canada (L.K.). The Biomolecular NMR Facility at the University of Western Ontario was supported by a Research Resource grant from the Canadian Institutes of Health Research (G.S.S.). N.M.M. holds Ontario Graduate Scholarship and London and Middlesex Alzheimer Awards. B.L.B. holds an NSERC CGS award.

* To whom correspondence should be addressed: Department of Biochemistry, University of Western Ontario, London, Ontario N6A 5C1, Canada. Phone: (519) 661-4021. Fax: (519) 661-3175. E-mail: gshaw1@uwo.ca.

[‡] Department of Biochemistry.

[§] Department of Chemistry.

10.1021/bi802086a CCC: $40.75
Published on Web 02/13/2009

addition, the dissociation constants of different S100 proteins have been shown to cover more than 3 orders of magnitude. For example, surface plasmon resonance experiments show rather low affinities for homodimeric S100P (K_{dimer}[1] $\sim 2\ \mu M$) (*28*) and S100A4 ($K_{dimer} \sim 4\ \mu M$) (*29*) and S100A1−S100P ($K_{dimer} \sim 1.8\ \mu M$) (*30*) or S100A9−S10012 ($K_{dimer} \sim 1.5\ \mu M$) (*31*) heterodimers. In contrast, the affinity for S100B dimerization appears to be much higher ($K_{dimer} < 1$ nM) since subunit dissociation was not observed during concentration-dependent gel filtration measurements (*32*).

Protein oligomerization can be dependent on a variety of factors such as ligand binding and ionic strength. Examples include β-lactoglobulin (*33*), formyltransferase (*34*), mitogen-activated protein kinase, ERK2 (*35*), stromal cell-derived factor 1 (*36*), and protein HU (*37*), all of which form monomers at low ionic strength but dimers at higher salt concentrations. Further, the structural characterization of folded monomeric subunits can provide important details about the mechanism for folding of dimeric proteins. Despite the potential functional relevance of S100 protein dimerization, the factors that influence their interactions have not been systematically explored yet. In this work, we examine the monomer−dimer equilibria of S100B and S100A11 as a function of ionic strength. Using nuclear magnetic resonance (NMR) spectroscopy as well as electrospray ionization mass spectrometry (ESI-MS), we show that the dimerization propensity of both proteins is strongly dependent on salt concentration. Specifically, a marked shift from the homodimeric to the monomeric forms was observed upon reduction of the ionic strength for both proteins. Our results are the first to demonstrate the formation of highly structured monomeric S100 proteins in solution, thereby providing important clues for the folding mechanism of these species. In addition, the isolation of folded monomers will facilitate future experiments aimed at establishing the propensity for homo- and heterodimer formation that may help identify the biological roles of these species.

EXPERIMENTAL PROCEDURES

Protein Expression, Labeling, and Purification. Expression and purification of human S100B and rabbit S100A11 were carried out as previously described (*13, 38, 39*). For S100A11, a C9S substitution (*40*) was used to prevent disulfide bond formation observed in both the crystal structure (*14*) and calcium binding experiments (*41*). Briefly, the two proteins were expressed from *Escherichia coli* strain N99 (S100B) or BL21(DE3) (S100A11) and purified using a combination of ammonium sulfate precipitation and either anion exchange (S100B) or phenyl-Sepharose (S100A11) chromatography. S100A11 yielded a single band by gel electrophoresis that was identified by ESI-MS ($MW_{obs} = 11283 \pm 1$ Da; $MW_{calc} = 11282$ Da). For S100B, a single band by gel electrophoresis was also observed, although this protein contains three chemically distinct forms. The three forms are the result of N-terminal modifications that have been characterized as formylmethionine S100B, desformylmethionine S100B, and desmethionine S100B (*42*). ESI-MS analysis of the samples employed for this study revealed formylmethionine S100B ($MW_{obs} = 10742 \pm 1$ Da; $MW_{calc} = 10740$ Da) to be the dominant form (ca. 50%), whereas the contributions of the other two species were approximately 40 and 10%, respectively (data not shown). For both S100A11 and S100B, no evidence of covalent dimer formation via disulfide formation was observed in mass spectral data under denaturing conditions. Following purification, S100B and S100A11 proteins were dialyzed against 3 mM KCl at pH 8.0 and freeze-dried. Initial protein stocks were created by weighing out freeze-dried ^{15}N-labeled or unlabeled protein and dissolving it in deionized water to a final concentration of ~2 mM. Actual protein concentrations were determined by amino acid analysis (Alberta Peptide Institute, Edmonton, AB) and done in triplicate using the peak areas for alanine and leucine. These stocks were used throughout this study where all protein concentrations will be reported on a per monomer basis.

Preparation of Low-Salt Protein Samples. Preparation of low-salt S100B and S100A11 samples was carried out using 250 μM protein solutions (prepared from the stock solutions described above) and extensive dialysis against 10 mM NH_4Ac (BDH Inc., Toronto, ON) at pH 7.5. After dialysis, the protein samples were freeze-dried and redissolved in water. This process was repeated twice to ensure extensive desalting of the samples, termed "low salt" throughout this work. Quantification of residual KCl was probed by inductively coupled plasma atomic emission spectroscopy (Laboratory of Biochemical Analysis, University of Western Ontario). This method revealed that the low-salt protein samples contained 40 μM potassium. The concentration of NH_4Ac was determined by ^{1}H NMR through comparison of the integrated peak area for acetate to that of an internal standard, DSS (2,2-dimethyl-2-silapentane-5-sulfonic acid). It was found that these samples contained <10 μM acetate. Hence, the total ionic strength for low-salt samples was ~50 μM for a 250 μM protein solution.

NMR Spectroscopy. All NMR experiments were conducted at 35 °C using a Varian Inova 600 MHz spectrometer equipped with a triple-resonance probe and z-field gradients. Sensitivity-enhanced ^{1}H−^{15}N HSQC spectra (*43*) for apo-S100B were acquired using carrier frequencies of 4.72 ppm (^{1}H) and 115.94 ppm (^{15}N) and spectral widths of 7000 and 1800 Hz, respectively. Similarly, spectra for apo-S100A11 were recorded by using identical carrier frequencies and spectral widths of 8000 Hz (^{1}H) and 1580 Hz (^{15}N). All data were processed using NMRPipe (*44*) and analyzed with NMRView (*45*). Sequential assignments of dimeric human apo-S100B (Protein Data Bank entry 2PRU) and dimeric rabbit apo-S100A11 (Protein Data Bank entry 1NSH) were completed on the basis of previously published data (*25, 39*). Chemical shift changes were expressed as

$$\Delta\delta = |\Delta\delta(^1\mathrm{H})| + 0.2|\Delta\delta(^{15}\mathrm{N})| \quad (1)$$

where $\Delta\delta(^1$H) and $\Delta\delta(^{15}$N) are the changes in backbone amide proton and nitrogen chemical shifts, respectively (*46*).

[1] Abbreviations: NMR, nuclear magnetic resonance; HSQC, heteronuclear single-quantum correlation; apo-S100B, calcium-free S100B protein; apo-S100A11, calcium-free S100A11 protein carrying a C9S substitution; K_{dimer}, dimer dissociation constant; CD, circular dichroism; ESI, electrospray ionization; MS, mass spectrometry; PFG, pulsed field gradient; R_h, radius of hydration; ASA, accessible surface area; NH_4Ac, ammonium acetate; DSS, 2,2-dimethyl-2-silapentane-5-sulfonic acid; ICP-AES, inductively coupled plasma atomic emission spectrometry; MW_{calc}, calculated molecular weight; MW_{obs}, observed molecular weight.

Dilution and Salt Titration Experiments. A series of sensitivity-enhanced $^1H-^{15}N$ HSQC spectra (*43*) were collected at monomer S100B and S100A11 concentrations of 250, 125, 60, and 30 μM. All protein samples were diluted with a stock solution of 60 mM NH_4Ac prepared in a 90% H_2O/10% D_2O mixture at pH 7.2. The number of transients was increased as concentrations were lowered to maintain an adequate signal-to-noise ratio.

$^1H-^{15}N$ HSQC spectra (*43*) were collected for both proteins over a range of NH_4Ac concentrations. Low-salt protein samples were prepared as described above in a 90% H_2O/10% D_2O solution at pH 6.8 (S100B) and pH 7.0 (S100A11). Small additions (1−2 μL) from stock solutions of either 60 mM or 6 M NH_4Ac were made directly to the NMR samples using a calibrated 10 μL Hamilton syringe. The pH of these samples was maintained throughout the salt series by adjusting the salt stock solutions to the pH of the protein solutions. Samples were equilibrated for 30 min at 35 °C prior to data acquisition.

Dissociation constants for the monomer−dimer equilibrium (K_{dimer}) were determined using eq 2

$$K_{dimer} = \frac{f_m^2 \times 2[P_t]}{1 - f_m} \quad (2)$$

where f_m is the fraction of monomeric protein at a given salt concentration and $[P_t]$ is the total protein concentration in terms of monomer. Under the fast exchange limit, f_m was calculated using eq 3 from the observed chemical shift at each salt concentration (δ_{obs}) and the corresponding data for the monomeric (δ_m) and dimeric proteins (δ_d) identified for each residue under low-salt and 40 mM NH_4Ac conditions, respectively.

$$\delta_{obs} = f_m\delta_m + (1 - f_m)\delta_d \quad (3)$$

Translational Diffusion Experiments. Translational diffusion coefficients were obtained at a protein concentration of 250 μM at low salt and 60 mM NH_4Ac concentrations using pulse field gradient water-suppressed longitudinal encode−decode (Water-SLED) experiments (*47*). Diffusion measurements were taken in triplicate using 0.03% dioxane as an internal standard. Peak integrals and intensities for protein and dioxane were extracted from the diffusion spectra and fit using GraphPad Prism (Macintosh version 4.0a) to the equation (*48*)

$$Y = A_o e^{-kg^2} \quad (4)$$

where A_o is the initial peak integral, Y is the integral of the signal at each gradient strength g^2, and k is the diffusion rate. Using the measured diffusion rates for the protein ($k_{protein}$) and the standard ($k_{dioxane}$) and the known radius of hydration (R_h) for dioxane (2.12 Å), the protein radius of hydration [$R_{h(protein)}$] was determined from eq 5 (*48, 49*).

$$R_{h(protein)} = 2.12\ \text{Å}(K_{dioxane}/K_{protein}) \quad (5)$$

In addition, the theoretical radii of hydration for dimeric S100B and S100A11 were calculated using Hydropro (version 7.c) (*50*) on the basis of the atomic coordinates of human apo-S100B (Protein Data Bank entry 2PRU) and rabbit apo-S100A11 (Protein Data Bank entry 1NSH). For monomeric versions of these proteins, the radii of hydration were calculated using chain A of the most representative structure from the Protein Data Bank entry.

Mass Spectrometry. Electrospray mass spectra were recorded on a Q-TOF Ultima API instrument (Waters/Micromass, Manchester, U.K.) utilizing a standard Z-spray ESI source operating in positive ion mode. All MS parameters were optimized to give the highest S100 dimer signal at pH 6.8 in the presence of NH_4Ac. A capillary voltage of 3.5 kV, a cone voltage of 45 V, and an RF lens 1 voltage of 20 V were found to be optimal. The desolvation and source temperatures were kept low (30 and 80 °C, respectively) to minimize dimer dissociation in the gas phase. Samples were introduced into the mass spectrometer at a flow rate of 5 μL/min via a syringe pump. All protein solutions were prepared to a concentration of 25 μM from low-salt lyophilized samples and analyzed under equilibrium conditions as aqueous NH_4Ac was titrated in. The mass spectrometer was calibrated with CsI and the ion optics adjusted to provide uniform transmission in the *m*/*z* range of interest. All data were acquired and analyzed using MassLynx provided by the instrument manufacturer.

Circular Dichroism. Samples were prepared by diluting a 2 mM stock solution of lyophilized S100B or S100A11 in water or 60 mM NH_4Ac (pH 6.8) to a final concentration of 40 μM. CD experiments were carried out at 35 °C on a Jasco (Easton, MD) J-810 spectropolarimeter using a 1 mm path length quartz cuvette and a scanning speed of 10 nm/min for 100 scans. CD samples were equilibrated at 35 °C for 30 min prior to each measurement. All spectra were baseline-subtracted using a matched buffer solution. Data are expressed as mean residue ellipticity [θ_m] (degrees square centimeter per decimole).

RESULTS AND DISCUSSION

Previous studies designed to examine the monomer−dimer equilibria for S100 proteins utilized surface plasmon resonance to characterize the dissociation and association processes (*28, 30, 31, 51*). Analytical gel filtration (*32*) has been used to determine the oligomerization state of S100B to show it has a >1000-fold higher dimerization affinity than either S100A4 or S100P. Those previous experiments did not allow the observation of structural changes that might occur upon dimer dissociation. In the work presented here, we examine the salt-dependent dimer−monomer equilibria for apo-S100B and apo-S100A11 and characterize the secondary and tertiary folds of the monomeric subunits.

Concentration-Dependent Chemical Shift Perturbations for Apo-S100 Proteins. To characterize the dimerization propensity of S100B and S100A11, we first investigated the structural changes that occur as a function of protein concentration. Calcium-free conditions were maintained throughout these experiments because previous studies on other S100 proteins found lower dimerization affinities in the absence of calcium (*29, 30, 52*). $^1H-^{15}N$ HSQC spectra were recorded for apo-S100B and apo-S100A11 over protein concentrations from 250 to 30 μM under constant solution conditions (60 mM NH_4Ac, 35 °C, and pH 7.2). The "volatile" salt NH_4Ac was used to control the ionic strength to allow a side-by-side comparison of NMR and ESI-MS data (see below). Control experiments monitored by NMR spectroscopy using 60 mM KCl instead of 60 mM NH_4Ac

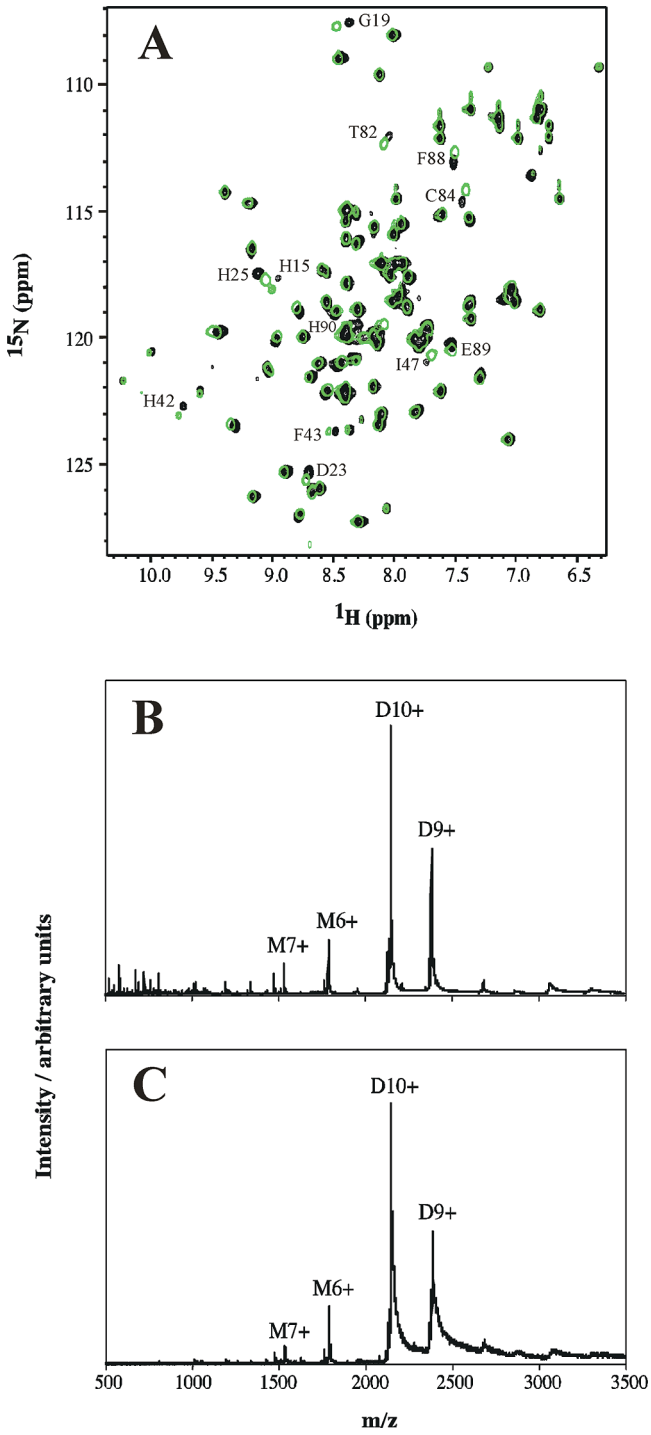

FIGURE 1: Concentration dependence of apo-S100B examined by NMR and ESI-MS. (A) $^{1}H-^{15}N$ HSQC spectra for apo-S100B (250 μM, black contours) and 30 μM (green contours). Residues with observable chemical shift changes are indicated. (B and C) ESI-MS spectra of apo-S100B recorded in positive ion mode at monomer protein concentrations of (B) 250 μM and (C) 1 μM. Charge states for the monomer (M) and dimer (D) are indicated. All samples were prepared in 60 mM NH_4Ac at pH 7.2.

revealed only small differences in chemical shifts, indicating that the choice of salt has little effect on the fold and oligomerization state of the protein (data not shown).

$^{1}H-^{15}N$ HSQC spectra of apo-S100B recorded at protein concentrations of 250 and 30 μM are shown in Figure 1A. Overall, the two data sets are very similar, although a few residues exhibit minor chemical shift changes. For example, residues in the first calcium-binding site (G19, D23, and H25), the linker region between helices II and III (H42, F43, and I47), and the C-terminus (C84, F88, E89, and H90) of apo-S100B showed small (<0.1 ppm) alterations in peak position. These changes are much smaller than those observed upon binding of calcium (*53*) and/or target proteins (*54*−*56*) to S100B, indicating that the backbone conformation of the protein is not significantly altered as the protein concentration is lowered. Apo-S100A11 showed even less pronounced concentration-dependent changes in analogous $^{1}H-^{15}N$ HSQC experiments (data not shown).

ESI-MS was used to examine the oligomerization state of apo-S100B and apo-S100A11. Data were recorded over the concentration range used in the NMR dilution series and extended to a lower limit of 1 μM. ESI mass spectra for apo-S100B at protein concentrations of 250 and 1 μM are shown in Figure 1B,C. Both spectra are strongly dominated by dimeric protein ions (labeled as D10+ and D9+), with only minor contributions arising from monomers (M7+ and M6+). These data confirm that S100B retains its dimeric structure over the concentration range studied here. Similar observations were made for S100A11 (not shown). These experiments show that the dissociation constant (K_{dimer}) for both apo-S100B and apo-S100A11 must be less than 1 μM under the conditions used here (60 mM NH_4Ac and pH 7.2). These findings are in agreement with previously published sedimentation equilibrium data (*57*) and analytical gel filtration experiments (*32*) which show that S100B retains its dimeric state above 1 μM protein.

S100 Dimer Dissociation at Low Ionic Strength. ESI-MS measurements carried out under nondenaturing solvent conditions represent a simple and effective way of tracking changes in the oligomerization state of proteins (*37, 58*−*61*). This method was employed here to study the effects of ionic strength on the monomer−dimer equilibria of apo-S100B and apo-S100A11 at a protein concentration of 25 μM (Figure 2). At 22 mM NH_4Ac, the spectra of both proteins are strongly dominated by dimers. Further addition of NH_4Ac to a concentration of 100 mM produced no changes in the spectra (not shown). These observations are consistent with the predominance of dimers seen at 60 mM NH_4Ac over the protein concentration range of 1−250 μM (Figure 1). Importantly, however, lowering the NH_4Ac concentration induces significant changes in the spectra (Figure 2). For S100B, low-salt samples were dominated by monomers (in charge states M6+ to M11+) with only very minor peaks from dimers (D9+ and D8+). Low-salt apo-S100A11 exhibited almost exclusively monomeric ions centered around M13+. These observations are consistent with the monomeric ions observed for apo-S100A4 under low-salt conditions (*29*), although S100A4 is complicated by the appearance of covalent disulfide-bonded dimers likely formed from the proximity of C76 across the dimer interface (*61*). Unlike S100A4, no evidence of disulfide-linked dimer formation was observed for apo-S100A11 or apo-S100B. Overall, the data in Figure 2 demonstrate that the dimerization propensity of apo-S100B and S100A11 is strongly dependent on ionic strength. This finding represents a key prerequisite for studying apo-S100B and apo-S100A11 in their monomeric states. In contrast, simple dilution experiments carried out at elevated ionic strengths (as in Figure 1) are not suitable for inducing dissociation of the complexes, at least not in

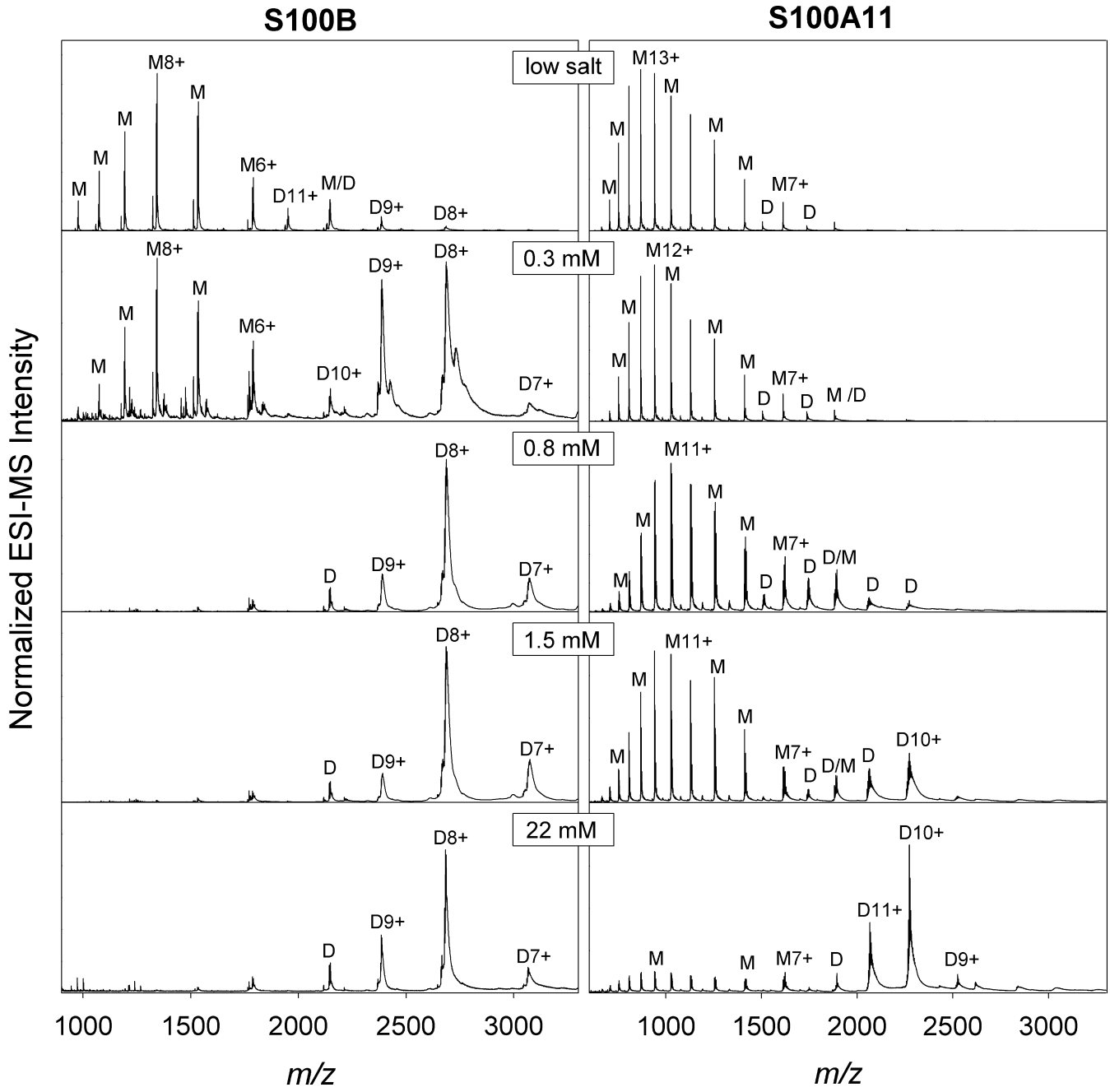

FIGURE 2: ESI mass spectra of apo-S100B (left) and apo-S100A11 (right) recorded at a protein concentration (based on monomer) of 25 μM in the presence of various concentrations of ammonium acetate. M and D represent monomeric and dimeric species, respectively. Also shown are the charge states (protonation states) of selected ions. Overlapping monomer/dimer peaks are denoted as M/D. Low salt refers to extensively desalted samples as described in the text. Slight shifts to lower protonation states with an increase in salt concentration are attributed to acetate-induced charge reduction, a phenomenon that is well-known in the ESI-MS literature (*70*).

the range of protein concentrations required for most biophysical methods.

Differences in the desolvation behavior and ionization efficiency (*62*) of monomeric and dimeric proteins make it difficult to accurately pinpoint the midpoints of the salt-induced transitions studied here. From the data depicted in Figure 2, it can be roughly estimated, however, that the midpoint for apo-S100B occurs around 0.3 mM NH_4Ac whereas the midpoint for apo-S100A11 occurs at NH_4Ac concentrations greater than 1.5 mM. Thus, apo-S100B has a greater propensity to dimerize than apo-S100A11. It is possible that this effect is due to differences in the architecture of the two binding interfaces. The interface of apo-S100B covers an area of ~1850 Å^2 per monomer, ~30% more than for apo-S100A11, where the interface surface area is ~1430 Å^2.

Monomeric Apo-S100B and Apo-S100A11 Retain a Compact α*-Helical Structure.* The ESI-MS data in Figure 2 revealed that apo-S100B and apo-S100A11 dissociate to their monomeric subunits at low ionic strength but retain dimeric structures at higher ionic strengths. We characterized the two proteins by far-UV CD to determine if dissociation leads to changes in secondary structure. For both proteins, CD spectra recorded under low-salt conditions and in 60 mM NH_4Ac are virtually identical. For example, apo-S100A11 had characteristic α-helical minima at 208 and 222 nm and a similar $\theta_{222}/\theta_{208}$ ratio of ~0.9 (Figure 3A) at both salt concentrations. This indicates that apo-S100A11 retains high

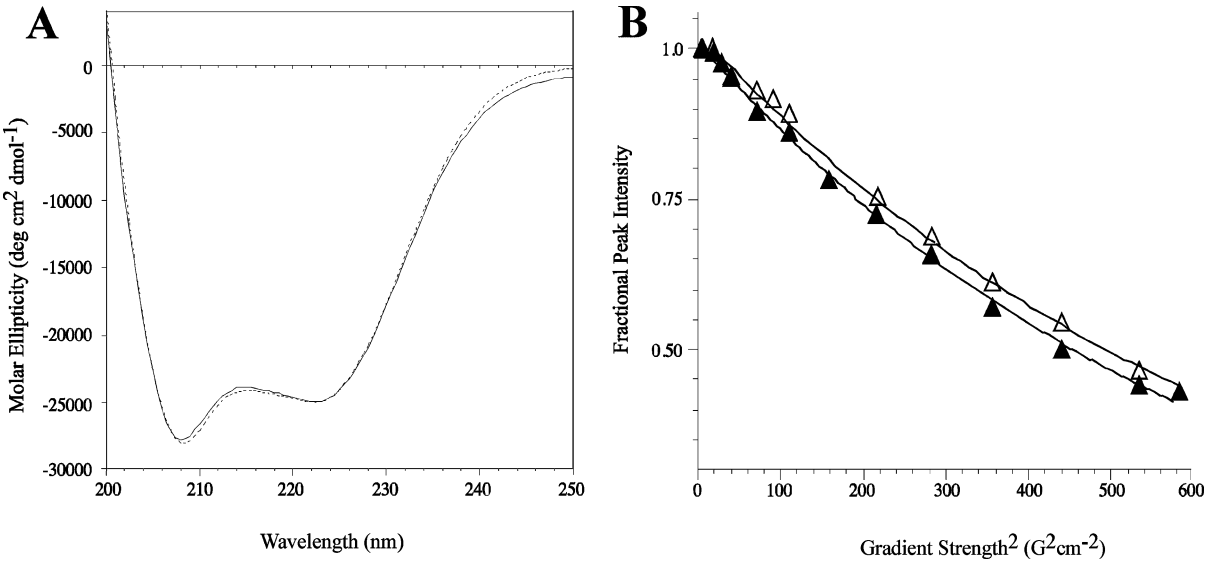

FIGURE 3: Effect of ionic strength on the secondary structure and hydrodynamic radius of apo-S100A11. (A) Far-UV CD spectrum for apo-S100A11 in the presence of 60 mM salt (—) and under low-salt conditions (---). (B) Fractional peak intensities for the methyl region of apo-S100A11 obtained from translational diffusion experiments under low-salt (▲) and 60 mM NH_4Ac (△) conditions. The curves shown for each data set are fitted according to eq 4 as described in Experimental Procedures. The data yielded radii of hydration for apo-S100A11 of 20.5 ± 0.4 Å under low-salt conditions and 24.7 ± 0.5 Å at 60 mM NH_4Ac.

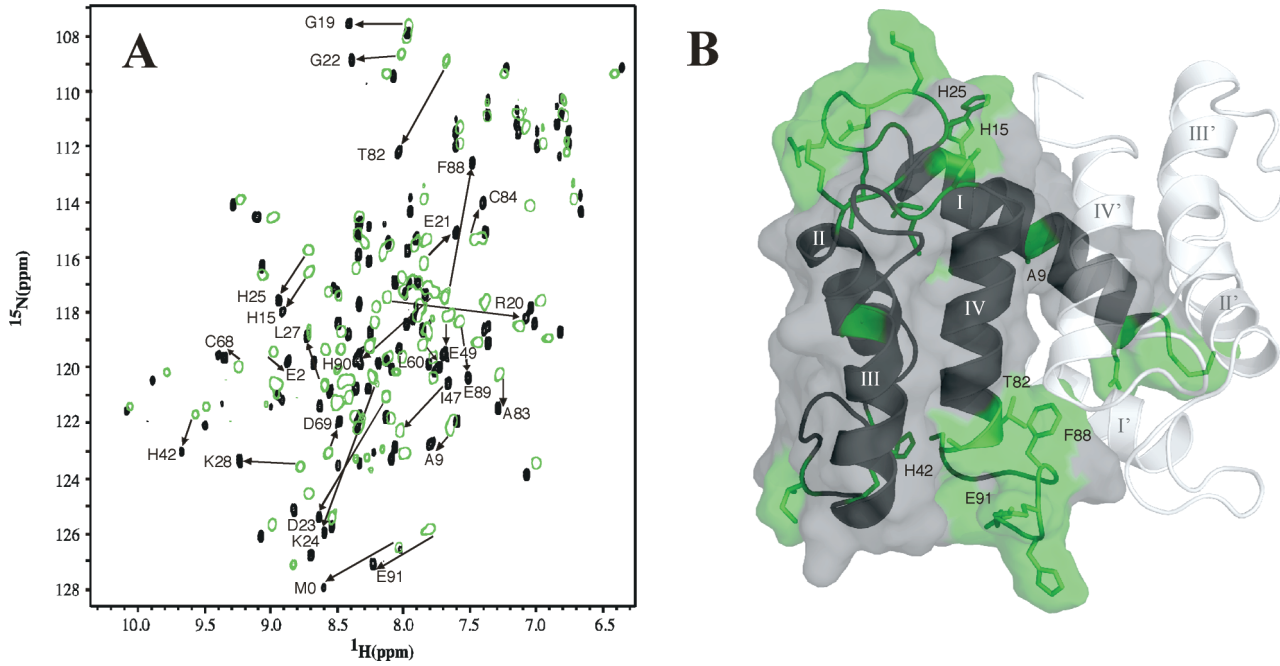

FIGURE 4: ^{1}H−^{15}N HSQC spectra showing the effect of ionic strength on the oligomerization state of apo-S100B. (A) ^{1}H−^{15}N HSQC spectra of apo-S100B (250 μM, monomer) at 60 mM NH_4Ac (black contours) and at low salt (green contours) at pH 6.8 and 35 °C. Residues that underwent significant chemical shift changes ($\Delta\delta$ > 0.25 ppm) as the ionic strength, and hence dimer population, was increased are indicated by arrows. (B) Structure of apo-S100B showing residues with the most significant chemical shift changes identified in panel A colored on the monomeric surface structure of apo-S100B.

α-helicity in its dimeric (high salt) and monomeric (low salt) states. A similar behavior has previously been observed for other proteins. For example, dimerization of stefin A (*63*) and GST-pi (*64*) is associated with only very small changes in the corresponding CD spectra, similar to the cases studied here.

The oligomerization states of apo-S100B and apo-S100A11 were also studied by translational diffusion experiments as a function of ionic strength. Under conditions where these proteins retain a dimeric structure (250 μM, in 60 mM NH_4Ac), the radius of hydration (R_h) for apo-S100A11 was 24.7 ± 0.5 Å (Figure 3B), close to that calculated for the dimeric form of the protein on the basis of its three-dimensional coordinates (23.6 Å) (*13*). Similarly, the measured R_h for apo-S100B was found to be 23.6 ± 0.4 Å, in excellent agreement with the Stokes radius (22.7 and 24.0 Å) determined by analytical gel filtration methods (*32, 65*) or the calculated value (*50*) of R_h (22.9 Å) based on the NMR structure (*25*). At low ionic strength, the translational diffusion data for both apo-S100B and apo-S100A11 yielded steeper curves compared to the curves from data measured at 60 mM NH_4Ac (Figure 3B). For both proteins, this yielded experimental R_h values of 20.5 ± 0.4 Å at low ionic strength. The smaller radii of hydration at low ionic strength are

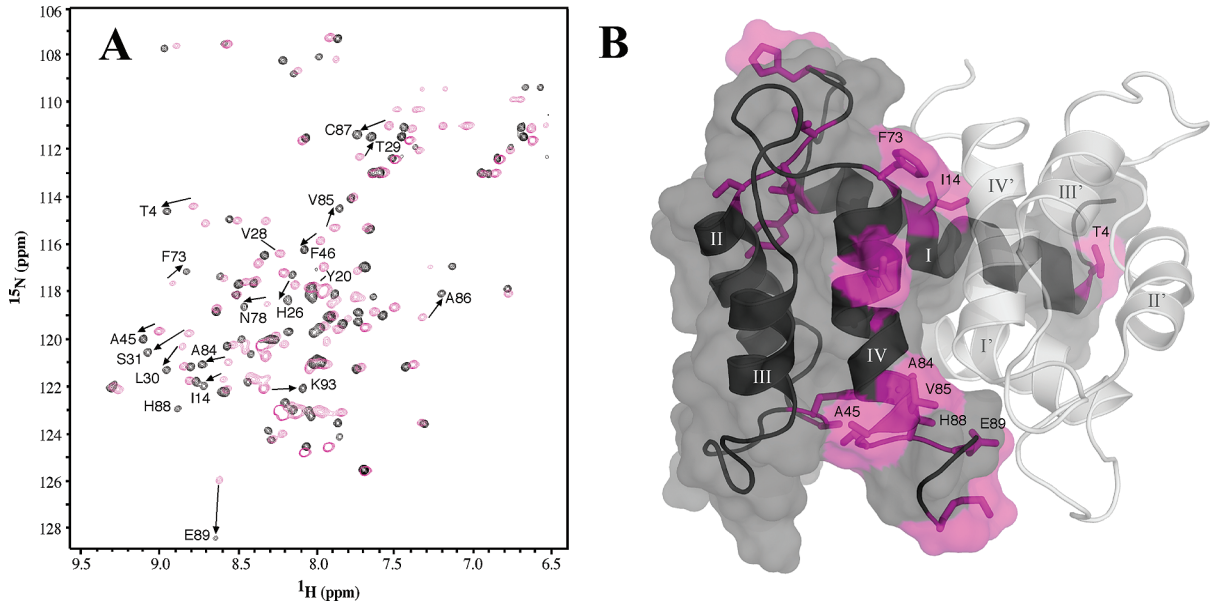

FIGURE 5: ^{1}H−^{15}N HSQC spectra showing the effect of ionic strength on the oligomerization state of apo-S100A11. (A) ^{1}H−^{15}N HSQC spectra of apo-S100A11 (250 μM, monomer) at 60 mM NH_4Ac (black contours) and at low salt (magenta contours) at pH 7.0 and 35 °C. (B) Structure of apo-S100A11 showing residues with the most significant chemical shift changes ($\Delta\delta$ > 0.16 ppm) identified in panel A colored on the monomeric surface structure of apo-S100A11.

consistent with dimer dissociation observed by ESI-MS (Figure 2). In agreement with this conclusion, the calculated values using the folded, monomeric subunits of the two proteins (S100B, 19.6 Å; S100A11, 20.9 Å) are close to the experimentally measured translational diffusion values. Notably, the measured R_h values are very distinct from those calculated (*49*) for unfolded monomeric S100B (28.9 Å) or S100A11 (30.7 Å), indicating that the dimer dissociation is not associated with global unfolding. The relatively high charge states seen for monomeric S100A11, however, suggest a certain degree of structural perturbation when compared with other proteins of similar size (*66*).

Influence of Ionic Strength on the S100 Tertiary Structure. The monomer−dimer transitions of apo-S100B and apo-S100A11 were examined by NMR spectroscopy to explore structural changes in more detail. Specifically, chemical shift perturbations were monitored by recording a series of ^{1}H−^{15}N HSQC spectra as a function of NH_4Ac concentration. For consistency, NMR titrations were conducted using solution conditions similar to those used for ESI-MS, albeit using a higher protein concentration (250 μM). Figures 4 and 5 show the ^{1}H−^{15}N HSQC spectra of apo-S100B and apo-S100A11 at low salt and in the presence of 60 mM NH_4Ac. There are very large differences in the resonance positions at the two ionic strengths. The alterations shown in Figures 4A and 5A correspond to average values ($\Delta\delta$) of 0.27 and 0.11 ppm for apo-S100B and apo-S100A11, respectively. The observed changes are more than 10-fold greater than those occurring upon dilution of the protein (Figure 1) and are more similar in magnitude to chemical shift changes accompanying calcium (*53*) or target protein binding (*54*−*56*). For example, residues D23, K24, T82, and F88 in apo-S100B change by nearly 5 ppm in the ^{15}N dimension upon addition of salt. Broad chemical shift dispersion is maintained under low-salt conditions for both proteins, and there is a minimum of line broadening indicating that the protein monomers retain a significant degree of tertiary structure. During the salt addition, all resonances in both proteins exchanged on the fast chemical shift time scale, allowing assignments to be performed on the basis of previously reported data for apo-S100B (*25*) and apo-S100A11 (*39*). In addition, we observed that all the low-salt resonance peaks tracked back to their previously assigned positions (at high ionic strength), indicating that ionic strength-induced structural changes are reversible.

To determine whether residues exhibiting the largest salt-dependent chemical shift changes correlate with the dimerization interfaces for apo-S100B and apo-S100A11, residues with $\Delta\delta$ values of >0.25 and >0.16 ppm were mapped onto the surface structures for apo-S100B (Figure 4B) and apo-S100A11 (Figure 5B), respectively. The figures show that 7 of 26 (apo-S100B) and 8 of 21 (apo-S100A11) interface-contributing residues display significant backbone chemical shift changes as the ionic strength is manipulated. There is good agreement for residues that change in chemical shift, and those at the dimer interface in helix I (T4 and I14, S100A11; E2, A9, and H15, S100B), helix IV (A84, H88, and E89, S100A11; T82 and F88, S100B), and the linker (A45 and F46, S100A11; H42, S100B). In both proteins, a notable shift is observed for V28 (S100A11) and H25 (S100B) in calcium-binding loop I that contacts the C-terminus of helix IV in the partner protomer. Although a continuous interface surface is not identified from these chemical shift changes, the majority of the shifting residues are concentrated near the dimer interface for apo-S100B and apo-S100A11. These observations are similar to those for tyrosine phosphatase and glutaredoxin, both of which display only eight significant chemical shift changes upon dimer dissociation, whereas the dimerization interface encompasses a several-fold larger number of residues (*67, 68*). Similarly, the dissociation of stromal cell-derived factor 1 (*36*) has been observed using concentration-dependent HSQC measurements, and also in that case, not all residues at the dimer interface underwent significant chemical shift changes. The broad chemical shift dispersion maintained by apo-S100B and apo-S100A11 under low-salt conditions (Figure 4A and

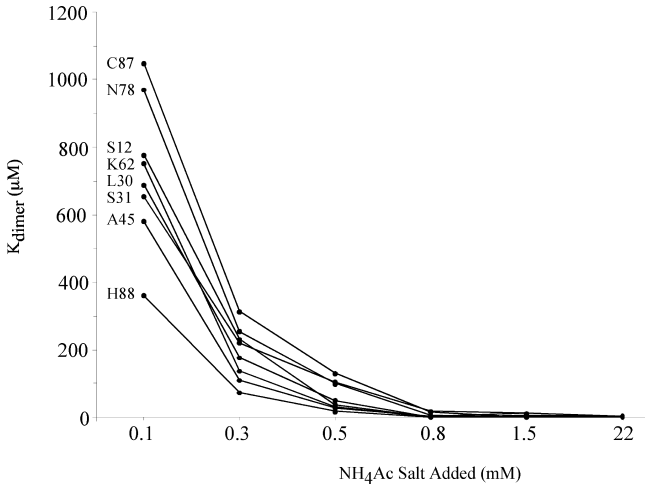

FIGURE 6: Salt-dependent dimerization constant (K_{dimer}) for apo-S100A11. For the residues indicated, K_{dimer} was determined using the fraction monomer calculated from the observed chemical shift at each NH_4Ac concentration. Details are provided in Experimental Procedures.

5A) indicates a significant portion of the tertiary structure of the monomeric proteins is preserved upon dimer dissociation.

Salt-dependent changes in chemical shift observed for apo-S100A11 are depicted in Figure 6 for selected residues. Using the observed chemical shift limits for the monomeric and dimeric states (Figure 5), we calculated K_{dimer} as a function of ionic strength. In the fast exchange limit encountered under the conditions of this work, the populations of monomer and dimer can be determined from a weighted chemical shift average (eq 3). Figure 6 confirms that there is an extreme dependence of K_{dimer} on ionic strength. Although the magnitude of K_{dimer} varied somewhat due to small variations in the chemical shifts for residues in the low-salt experiments, all signals exhibit a similar trend. At the lowest salt concentration of 0.1 mM NH_4Ac, the observed K_{dimer} ranges between 400 and 1000 μM. These observations are in agreement with our mass spectral data (Figure 2) that show apo-S100A11 at 25 μM to be essentially monomeric. At higher salt concentrations, K_{dimer} progressively decreases, reaching values near 0.01 μM for many of the residues shown in Figure 6 at 22 mM NH_4Ac. For apo-S100B, the salt-dependent changes in chemical shift were very severe, especially at the lowest salt concentrations used. This was not surprising on the basis of the extreme salt dependency for dimer formation for apo-S100B identified in mass spectral analysis (Figure 2). As a result, the identification of "monomeric" chemical shifts for apo-S100B was not possible and did not allow K_{dimer} to be determined by this method. Nevertheless, it is very clear from these data, and the salt dependency of mass spectral data presented in Figure 2, that apo-S100B has a much stronger tendency to dimerize than apo-S100A11.

CONCLUSIONS

Despite a wealth of structural data on S100 proteins, the role of dimerization for their functions is still not clear. The dimerization of S100 proteins is also linked to calcium binding and calcium affinities. For example, the dimerization affinities for S100A1−S100P (*30*), S100P (*28*), and S100A4 (*29*) are all ~2 orders of magnitude higher in the calcium-bound state than in the absence of calcium. In this work, we have shown that apo-S100B and apo-S100A11 dimers dissociate into compact α-helical monomers under low-ionic strength conditions. The monomeric species generated in this way retain a significant degree of tertiary structure. This observation is similar to those made for a wide variety of other protein systems. For example, the DNA-binding protein HU is monomeric at low NH_4Ac concentrations and forms dimers with an increase in ionic strength (*37*). In the same way, formyltransferase becomes tetrameric when salt concentrations exceed 300 mM (*34*). The dimerization of EF-hand peptides, representing a single calcium-binding site, can also be induced upon addition of salt (*69*). The observation that apo-S100A11 and apo-S100B can form folded monomeric subunits indicates that these monomers may be involved in the assembly of homo- and heterodimeric proteins. Indeed, evidence of the formation of a monomeric intermediate during the refolding of acid-denatured S100A11 comes from recent kinetic ESI-MS experiments (*40*).

Our work is the first to show that two different S100 proteins have distinguishable propensities to dimerize under similar conditions. Under low-salt conditions, the K_{dimer} for apo-S100A11 is estimated to be more than 400 μM from the data depicted in Figure 6. At higher ionic strengths, the dissociation constant for apo-S100A11 is near 0.01 μM (Figure 6). Apo-S100B appears to have a K_{dimer} at least 1 order of magnitude smaller than these values on the basis of its greater sensitivity to salt concentration observed in ESI-MS data (Figure 2) and NMR spectra (Figure 4). Thus, the binding affinities of these S100 proteins can be varied by several orders of magnitude through manipulation of ionic strength. Further, the differences in dimerization propensity for apo-S100A11 and apo-S100B along with previous measurements indicate that a wide range of dimer stabilities may exist for the S100 proteins. Apo-S100A11 appears to be of intermediate stability between apo-S100A4 and apo-S100P ($K_{dimer} \sim 2-4$ μM) (*28, 29*), whereas the K_{dimer} for apo-S100B is clearly much lower (*32*). The relative affinities of these proteins are in line with the buried interface surface area which shows apo-S100B has the greatest buried area (1850 Å^2 per monomer), that of apo-S100A11 is intermediate (1430 Å^2), and apo-S100A4 and apo-S100P have the smallest buried surface (~1350 Å^2). The extreme sensitivity of the dimerization affinity toward ionic strength is consistent with the mostly hydrophobic makeup of the dimer interface in the S100 proteins. Since the dimerization of S100 proteins may be linked to the regulation of their function, the isolation of folded monomers will allow future experiments to probe target binding and possible modulation of calcium affinity as a function of oligomerization state. Those future studies should shed light on the possible role of monomeric S100 subunits in calcium signaling.

ACKNOWLEDGMENT

We thank Qin Liu for maintenance of the Biomolecular NMR Facility and Lee-Ann Briere for help with CD spectra. We also thank Frank Delaglio for the program NMRPipe, Bruce Johnson for NMRView, and Andy Byrd (National Cancer Institute) for the Water-SLED pulse sequence used for translational diffusion measurements.

REFERENCES

1. Santamaria-Kisiel, L., Rintala-Dempsey, A. C., and Shaw, G. S. (2006) Calcium-dependent and -independent interactions of the S100 protein family. *Biochem. J. 396*, 201–214.
2. Marenholz, I., Heizmann, C. W., and Fritz, G. (2004) S100 proteins in mouse and man: From evolution to function and pathology (including an update of the nomenclature). *Biochem. Biophys. Res. Commun. 322*, 1111–1122.
3. Ferguson, P. L., and Shaw, G. S. (2004) Human S100B protein interacts with the *Escherichia coli* division protein FtsZ in a calcium-sensitive manner. *J. Biol. Chem. 279*, 18806–18813.
4. Frizzo, J. K., Tramontina, F., Bortoli, E., Gottfried, C., Leal, R. B., Lengyel, I., Donato, R., Dunkley, P. R., and Goncalves, C. A. (2004) S100B-mediated inhibition of the phosphorylation of GFAP is prevented by TRTK-12. *Neurochem. Res. 29*, 735–740.
5. Garbuglia, M., Verzini, M., Rustandi, R. R., Osterloh, D., Weber, D. J., Gerke, V., and Donato, R. (1999) Role of the C-terminal extension in the interaction of S100A1 with GFAP, tubulin, the S100A1- and S100B-inhibitory peptide, TRTK-12, and a peptide derived from p53, and the S100A1 inhibitory effect on GFAP polymerization. *Biochem. Biophys. Res. Commun. 254*, 36–41.
6. Li, Z. H., and Bresnick, A. R. (2006) The S100A4 metastasis factor regulates cellular motility via a direct interaction with myosin-IIA. *Cancer Res. 66*, 5173–5180.
7. Isobe, T., Ishioka, N., Masuda, T., Takahashi, Y., Ganno, S., and Okuyama, T. (1983) A rapid separation of S100 subunits by high performance liquid chromatography: The subunit compositions of S100 proteins. *Biochem. Int. 6*, 419–426.
8. Zwadlo, G., Bruggen, J., Gerhards, G., Schlegel, R., and Sorg, C. (1988) Two calcium-binding proteins associated with specific stages of myeloid cell differentiation are expressed by subsets of macrophages in inflammatory tissues. *Clin. Exp. Immunol. 72*, 510–515.
9. Drohat, A. C., Baldisseri, D. M., Rustandi, R. R., and Weber, D. J. (1998) Solution structure of calcium-bound rat S100B($\beta\beta$) as determined by nuclear magnetic resonance spectroscopy. *Biochemistry 37*, 2729–2740.
10. Drohat, A. C., Tjandra, N., Baldisseri, D. M., and Weber, D. J. (1999) The use of dipolar couplings for determining the solution structure of rat apo-S100B($\beta\beta$). *Protein Sci. 8*, 800–809.
11. Kilby, P. M., Van Eldik, L. J., and Roberts, G. C. (1996) The solution structure of the bovine S100B protein dimer in the calcium-free state. *Structure 4*, 1041–1052.
12. Smith, S. P., and Shaw, G. S. (1998) A novel calcium-sensitive switch revealed by the structure of human S100B in the calcium-bound form. *Structure 6*, 211–222.
13. Dempsey, A. C., Walsh, M. P., and Shaw, G. S. (2003) Unmasking the annexin I interaction from the structure of Apo-S100A11. *Structure (Cambridge, MA, U.S.) 11*, 887–897.
14. Rety, S., Osterloh, D., Arie, J. P., Tabaries, S., Seeman, J., Russo-Marie, F., Gerke, V., and Lewit-Bentley, A. (2000) Structural basis of the Ca^{2+}-dependent association between S100C (S100A11) and its target, the N-terminal part of annexin I. *Structure 8*, 175–184.
15. Otterbein, L. R., Kordowska, J., Witte-Hoffmann, C., Wang, C. L., and Dominguez, R. (2002) Crystal structures of S100A6 in the Ca^{2+}-free and Ca^{2+}-bound states: The calcium sensor mechanism of S100 proteins revealed at atomic resolution. *Structure (Cambridge, MA, U.S.) 10*, 557–567.
16. Sastry, M., Ketchem, R. R., Crescenzi, O., Weber, C., Lubienski, M. J., Hidaka, H., and Chazin, W. J. (1998) The three-dimensional structure of Ca^{2+}-bound calcyclin: Implications for Ca^{2+}-signal transduction by S100 proteins. *Structure (Cambridge, MA, U.S.) 6*, 223–231.
17. Maler, L., Potts, B. C., and Chazin, W. J. (1999) High resolution solution structure of apo calcyclin and structural variations in the S100 family of calcium-binding proteins. *J. Biomol. NMR 13*, 233–247.
18. Potts, B. C. M., Smith, J., Akke, M., Macke, T. J., Okazaki, K., Hidaka, H., Case, D. A., and Chazin, W. J. (1995) The structure of calcyclin reveals a novel homodimeric fold for S100 Ca^{2+}-binding proteins. *Nat. Struct. Biol. 2*, 790–796.
19. Matsumura, H., Shiba, T., Inoue, T., Harada, S., and Kai, Y. (1998) A novel mode of target recognition suggested by the 2.0 Å structure of holo S100B from bovine brain. *Structure 6*, 233–241.
20. Maler, L., Sastry, M., and Chazin, W. J. (2002) A structural basis for S100 protein specificity derived from comparative analysis of apo and Ca^{2+}-calcyclin. *J. Mol. Biol. 317*, 279–290.
21. Arnesano, F., Banci, L., Bertini, I., Fantoni, A., Tenori, L., and Viezzoli, M. S. (2005) Structural interplay between calcium(II) and copper(II) binding to S100A13 protein. *Angew. Chem., Int. Ed. 44*, 6341–6344.
22. Li, M., Zhang, P. F., Pan, X. W., and Chang, W. R. (2007) Crystal structure study on human S100A13 at 2.0 Å resolution. *Biochem. Biophys. Res. Commun. 356*, 616–621.
23. Imai, F. L., Nagata, K., Yonezawa, N., Nakano, M., and Tanokura, M. (2008) Structure of calcium-bound human S100A13 at pH 7.5 at 1.8 Å resolution. *Acta Crystallogr. F64*, 70–76.
24. Ferguson, P. L., and Shaw, G. S. (2002) Role of the N-terminal Helix I for dimerization and stability of the calcium-binding protein S100B. *Biochemistry 41*, 3637–3646.
25. Malik, S., Revington, M., Smith, S. P., and Shaw, G. S. (2008) Analysis of the structure of human apo-S100B at low temperature indicates a unimodal conformational distribution is adopted by calcium-free S100 proteins. *Proteins 73*, 28–42.
26. Deloulme, J. C., Gentil, B. J., and Baudier, J. (2003) Monitoring of S100 homodimerization and heterodimeric interactions by the yeast two-hybrid system. *Microsc. Res. Tech. 60*, 560–568.
27. Deloulme, J. C., Assard, N., Mbele, G. O., Mangin, C., Kuwano, R., and Baudier, J. (2000) S100A6 and S100A11 are specific targets of the calcium- and zinc-binding S100B protein in vivo. *J. Biol. Chem. 275*, 35302–35310.
28. Zhang, H., Wang, G., Ding, Y., Wang, Z., Barraclough, R., Rudland, P. S., Fernig, D. G., and Rao, Z. (2003) The crystal structure at 2 Å resolution of the Ca^{2+}-binding protein S100P. *J. Mol. Biol. 325*, 785–794.
29. Tarabykina, S., Scott, D. J., Herzyk, P., Hill, T. J., Tame, J. R., Kriajevska, M., Lafitte, D., Derrick, P. J., Dodson, G. G., Maitland, N. J., Lukanidin, E. M., and Bronstein, I. B. (2001) The dimerization interface of the metastasis-associated protein S100A4 (Mts1): In vivo and in vitro studies. *J. Biol. Chem. 276*, 24212–24222.
30. Wang, G., Zhang, S., Fernig, D. G., Spiller, D., Martin-Fernandez, M., Zhang, H., Ding, Y., Rao, Z., Rudland, P. S., and Barraclough, R. (2004) Heterodimeric interaction and interfaces of S100A1 and S100P. *Biochem. J. 382*, 375–383.
31. Hatakeyama, T., Okada, M., Shimamoto, S., Kubota, Y., and Kobayashi, R. (2004) Identification of intracellular target proteins of the calcium-signaling protein S100A12. *Eur. J. Biochem. 271*, 3765–3775.
32. Drohat, A. C., Nenortas, E., Beckett, D., and Weber, D. J. (1997) Oligomerization state of S100B at nanomolar concentration determined by large-zone analytical gel filtration chromatography. *Protein Sci. 6*, 1577–1582.
33. Sakurai, K., Oobatake, M., and Goto, Y. (2001) Salt-dependent monomer-dimer equilibrium of bovine β-lactoglobulin at pH 3. *Protein Sci. 10*, 2325–2335.
34. Shima, S., Tziatzios, C., Schubert, D., Fukada, H., Takahashi, K., Ermler, U., and Thauer, R. K. (1998) Lyotropic-salt-induced changes in monomer/dimer/tetramer association equilibrium of formyltransferase from the hyperthermophilic *Methanopyrus kandleri* in relation to the activity and thermostability of the enzyme. *Eur. J. Biochem. 258*, 85–92.
35. Wilsbacher, J. L., Juang, Y. C., Khokhlatchev, A. V., Gallagher, E., Binns, D., Goldsmith, E. J., and Cobb, M. H. (2006) Characterization of mitogen-activated protein kinase (MAPK) dimers. *Biochemistry 45*, 13175–13182.
36. Veldkamp, C. T., Peterson, F. C., Pelzek, A. J., and Volkman, B. F. (2005) The monomer-dimer equilibrium of stromal cell-derived factor-1 (CXCL 12) is altered by pH, phosphate, sulfate, and heparin. *Protein Sci. 14*, 1071–1081.
37. Vis, H., Heinemann, U., Dobson, C. M., and Robinson, C. V. (1998) Detection of a Monomeric Intermediate Associated with Dimerization of Protein Hu by Mass Spectrometry. *J. Am. Chem. Soc. 120*, 6427–6428.
38. Smith, S. P., Barber, K. R., Dunn, S. D., and Shaw, G. S. (1996) Structural influence of cation binding to recombinant human brain S100b: Evidence for calcium-induced exposure of a hydrophobic surface. *Biochemistry 35*, 8805–8814.
39. Rintala, A. C., Schonekess, B. O., Walsh, M. P., and Shaw, G. S. (2002) ^{1}H, ^{15}N and ^{13}C resonance assignments of rabbit apo-S100A11. *J. Biomol. NMR 22*, 191–192.
40. Pan, J., Rintala-Dempsey, A. C., Li, Y., Shaw, G. S., and Konermann, L. (2006) Folding kinetics of the S100A11 protein dimer studied by time-resolved electrospray mass spectrometry and pulsed hydrogen-deuterium exchange. *Biochemistry 45*, 3005–3013.

41. Rintala-Dempsey, A. C., Santamaria-Kisiel, L., Liao, Y., Lajoie, G., and Shaw, G. S. (2006) Insights into S100 target specificity examined by a new interaction between S100A11 and annexin A2. *Biochemistry 45*, 14695–14705.
42. Smith, S. P., Barber, K. R., and Shaw, G. S. (1997) Identification and structural influence of a differentially modified N-terminal methionine in human S100b. *Protein Sci. 6*, 1110–1113.
43. Kay, L. E., Keifer, P., and Saarinen, T. (1992) Pure absorption gradient enhanced heteronuclear single quantum correlation spectroscopy with improved sensitivity. *J. Am. Chem. Soc. 114*, 10663–10665.
44. Delaglio, F., Grzesiek, S., Vuister, G. W., Zhu, G., Pfeifer, J., and Bax, A. (1995) NMRPipe: A multidimensional spectral processing system based on UNIX pipes. *J. Biomol. NMR 6*, 277–293.
45. Johnson, B. A., and Belvins, R. A. (1994) NMRView: A computer program for the visualization and analysis of NMR data. *J. Biomol. NMR 4*, 603–614.
46. Shuker, S. B., Hajduk, P. J., Meadows, R. P., and Fesik, S. W. (1996) Discovering high-affinity ligands for proteins: SAR by NMR. *Science 274*, 1531–1534.
47. Altieri, A. S., Hinton, D. P., and Byrd, R. A. (1995) Association of biomolecular systems via pulsed field gradient NMR self-diffusion measurements. *J. Am. Chem. Soc. 117*, 7566–7567.
48. Jones, J. A., Wilkins, D. K., Smith, L. J., and Dobson, C. M. (1997) Characterisation of protein unfolding by NMR diffusion measurements. *J. Biomol. NMR 10*, 199–203.
49. Wilkins, D. K., Grimshaw, S. B., Receveur, V., Dobson, C. M., Jones, J. A., and Smith, L. J. (1999) Hydrodynamic radii of native and denatured proteins measured by pulse field gradient NMR techniques. *Biochemistry 38*, 16424–16431.
50. Garcia De La Torre, J., Huertas, M. L., and Carrasco, B. (2000) Calculation of hydrodynamic properties of globular proteins from their atomic-level structure. *Biophys. J. 78*, 719–730.
51. Wang, G., Zhang, S., Fernig, D. G., Martin-Fernandez, M., Rudland, P. S., and Barraclough, R. (2005) Mutually antagonistic actions of S100A4 and S100A1 on normal and metastatic phenotypes. *Oncogene 24*, 1445–1454.
52. Koltzscher, M., and Gerke, V. (2000) Identification of hydrophobic amino acid residues involved in the formation of S100P homodimers in vivo. *Biochemistry 39*, 9533–9539.
53. Smith, S. P., and Shaw, G. S. (1997) Assignment and secondary structure of calcium-bound human S100B. *J. Biomol. NMR 10*, 77–88.
54. Barber, K. R., McClintock, K. A., Jamieson, G. A., Jr., Dimlich, R. V., and Shaw, G. S. (1999) Specificity and Zn^{2+} enhancement of the S100B binding epitope TRTK-12. *J. Biol. Chem. 274*, 1502–1508.
55. Bhattacharya, S., Large, E., Heizmann, C. W., Hemmings, B., and Chazin, W. J. (2003) Structure of the Ca^{2+}/S100B/NDR kinase peptide complex: Insights into S100 target specificity and activation of the kinase. *Biochemistry 42*, 14416–14426.
56. Rustandi, R. R., Baldisseri, D. M., Drohat, A. C., and Weber, D. J. (1999) Structural changes in the C-terminus of Ca^{2+}-bound rat S100B($\beta\beta$) upon binding to a peptide derived from the C-terminal regulatory domain of p53. *Protein Sci. 8*, 1743–1751.
57. Mani, R. J. (1982) Physiochemical and optical studies on calcium- and potassium-induced conformational changes in bovine brain S-100b protein. *Biochemistry 21*, 2607–2612.
58. Heck, A. J. R., and Van den Heuvel, R. H. H. (2004) Investigation of intact protein complexes by mass spectrometry. *Mass Spectrom. Rev. 23*, 368–389.
59. Loo, J. A. (1997) Studying noncovalent protein complexes by electrospray ionization mass spectrometry. *Mass Spectrom. Rev. 16*, 1–23.
60. Boys, B. L., Kuprowski, M. C., and Konermann, L. (2007) Symmetric Behaviour of Hemoglobin α- and β-Subunits during Acid-Induced Denaturation Observed by Electrospray Mass Spectrometry. *Biochemistry 46*, 10675–10684.
61. Burkitt, W. I., Derrick, P. J., Lafitte, D., and Bronstein, I. (2003) Protein-ligand and protein-protein interactions studied by electrospray ionization and mass spectrometry. *Biochem. Soc. Trans. 31*, 985–989.
62. Kuprowski, M. C., Boys, B. L., and Konermann, L. (2007) Analysis of Protein Mixtures by Electrospray Mass Spectrometry: Effects of Conformation and Desolvation Behavior on the Signal Intensities of Hemoglobin Subunits. *J. Am. Soc. Mass Spectrom. 18*, 1279–1285.
63. Jerala, R., and Zerovnik, E. (1999) Accessing the global minimum conformation of stefin A dimer by annealing under partially denaturing conditions. *J. Mol. Biol. 291*, 1079–1089.
64. Huang, Y. C., Misquitta, S., Blond, S. Y., Adams, E., and Colman, R. F. (2008) Catalytically Active Monomer of Glutathione S-Transferase π and Key Residues Involved in the Electrostatic Interaction between Subunits. *J. Biol. Chem. 283*, 32880–32888.
65. Mani, R. S., and Kay, C. M. (1984) Hydrodynamic properties of bovine brain S-100 proteins. *FEBS Lett. 166*, 258–262.
66. Kaltashov, I. A., and Eyles, S. J. (2002) Studies of Biomolecular Conformations and Conformational Dynamics by Mass Spectrometry. *Mass Spectrom. Rev. 21*, 37–71.
67. Akerud, T., Thulin, E., Van Etten, R. L., and Akke, M. (2002) Intramolecular dynamics of low molecular weight protein tyrosine phosphatase in monomer-dimer equilibrium studied by NMR: A model for changes in dynamics upon target binding. *J. Mol. Biol. 322*, 137–152.
68. Noguera, V., Walker, O., Rouhier, N., Jacquot, J. P., Krimm, I., and Lancelin, J. M. (2005) NMR reveals a novel glutaredoxin-glutaredoxin interaction interface. *J. Mol. Biol. 353*, 629–641.
69. Julenius, K., Robblee, J., Thulin, E., Finn, B. E., Fairman, R., and Linse, S. (2002) Coupling of ligand binding and dimerization of helix-loop-helix peptides: Spectroscopic and sedimentation analyses of calbindin D9k EF-hands. *Proteins 47*, 323–333.
70. Mirza, U. A., and Chait, B. T. (1994) Effects of anions on the positive ion electrospray ionization mass spectra of peptides and proteins. *Anal. Chem. 66*, 2898–2904.

BI802086A